Available online at www.sciencedirect.com

ScienceDirect

Procedia CIRP 65 (2017) 19 – 24

www.elsevier.com/locate/procedia

3rd CIRP Conference on BioManufacturing

Micro-structuring of titanium collectors by laser ablation technique: a promising approach to produce micro-patterned scaffolds for tissue engineering applications

P. Ginestra[a*], A. Fiorentino[a], E. Ceretti[a]

Department of Mechanical and Industrial Engineering- University of Brescia – Via Branze 38, 25123 Brescia - Italy

* Corresponding author. Tel.: +390303715538; *E-mail address:* paolaserena.ginestra@gmail.com

Abstract

Multi-scale micro-structured scaffolds can sustain attachment and orientation of different cells phenotypes. An innovative use of laser ablation technique to build micro-structured titanium surfaces to be used as collectors in both electrophoretic deposition and electrospinning processes was investigated. To produce micro-patterned scaffolds, a negative replica patterning was exploited by designing specific patterns to be laser ablated on titanium plates. This method allows the deposition of the scaffolds on the mold, thus reproducing the micro-features on the scaffold surface. The titanium surface morphology depending on ablation parameters was studied and the capability of the process in replicating the micro-pattern was characterized.

Peer-review under responsibility of the scientific committee of the 3rd CIRP Conference on BioManufacturing 2017

Keywords: Patterning, laser ablation, electrospinning, electrophoresis, polymers.

1. Introduction

In medical device industry surfaces are the primary place of contact between biomaterial and organism. In this environment the need to design and manufacture materials to make them highly compatible with living tissue (including bio fluids such as blood) has become a major priority [1,2]. Direct fabrication of a scaffold mimicking the structure and functions of heart and skeletal muscle tissues from raw synthetic or biological materials is an approach distinct from decellularization of biological scaffolds [3,4]. In addition, morphology configuration and mechanical properties of these scaffolds can be controlled. The disadvantages are that their structure may not fully mimic the complexity of the native tissue with varied mechanical properties [5].

Regarding the scaffold, material selection and scaffold fabrication techniques are key points. The material utilized in producing cellular supports must be biocompatible with cell attachment sites [6]. Further, scaffold morphology can affect cellular adhesion and differentiation in a particular phenotype [7]. In particular, an interconnected porous structure allows nutrients and waste cellular product exchanges and a two-dimensional micro-pattern shape may play a role in controlling cellular morphology of embryonic stem cells [8].

In electrospinning and electrophoretic deposition tests a metal collector is used for the deposition of fibers and hydrogels [9,10,11]. Several approaches have been used to produce scaffolds with a controlled structure by the application of an external electrical field and by replacing the traditional two-dimensional (2D) plates collectors with rotating metallic mandrels or metal rings [12,13]. Recently, scaffolds with precise architectures and patterns have been produced by using wire meshes and drilling structures on metallic plates that were accurately mimicked in the resulting collected scaffolds [14]. Despite these advances, these new approaches are relatively slow and not fully reproducible experimental techniques. Moreover, the identification of a flexible and scalable method to design and fabricate collector plates with accurately controlled structures remains a challenge. Furthermore, the possibilities to scale-up manufacture of patterned scaffolds using these methods

Peer-review under responsibility of the scientific committee of the 3rd CIRP Conference on BioManufacturing 2017
doi:10.1016/j.procir.2017.04.043

could be limited. For these reasons, techniques that allow the design of collector plates with precise structures according to the specific requirements of the end-user, have to be combined with electrospinning and electrophoretic deposition to collect scaffolds with well defined micro-topography at the surface. Novel collector geometries with complex 3D structures have been designed and produced by additive manufacturing techniques and combined with electrospinning to obtain scaffolds consisting of both random fibres and a defined 3D micro-topography at the surface [15,16].

The manufacturing of periodic surface topography on the collector may be executed using lasers with medium power density (from W/cm^2 to MW/cm^2) [17]. This method allows to form micro- and sub- micrometer structures with well defined long range ordering [18].

In this paper, laser ablated titanium collectors are used as molds during electrospinning and electrophoretic deposition tests to produce scaffolds with a surface topography that replicates the ablated micro-pattern geometry. The influence of the patterns on cellular attachment and orientation was evaluated.

2. Pattern design and laser process

2.1. Definition of the geometry

A total of five pattern configurations were considered: three patterns for the electrospinning tests (ES), namely A, B and C (Fig.1) and two patterns for the electrophoretic deposition tests (EPD), namely D and E (Fig.2).

Configurations A, B and C are characterized by grooves having three different pitches (d_0) equal to 25 µm, 50 µm and 75 µm respectively.

The grooves of the configurations D and E are characterized by dimensions of 125 µm x 250 (l x L) defining rectangular structures. The whole pattern of each configuration has a 5x5 mm^2 area.

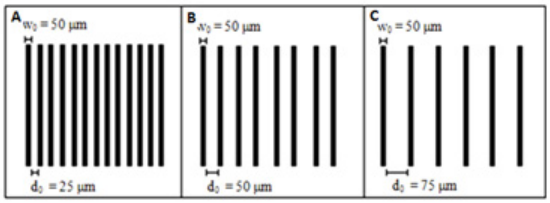

Fig. 1. Imposed pattern configurations A, B and C.

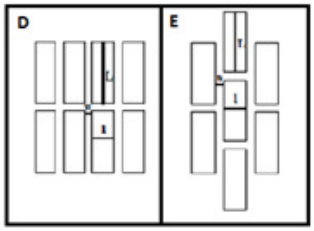

Fig. 2. Imposed pattern configurations D and E.

2.2. Laser ablation

The Titanium patterns (Ti CP Gr2) for ES and EDP application were realized by a laser micro-structuring process, using a LEP Lee Laser (Nd:YVO4, 8 W q-switched, λ=532 nm) for the laser ablation of flat collectors 0.5 mm thick. The laser machine is controlled by a software where it is possible to set the q-switch frequency, the duty cycle, the laser path strategy and the loop number of cycles of ablation. The high quality beam (M^2=1) can work at pulse frequency of 200 kHz and pulse minimum duration of 12 ns.

Pure Argon was chosen as assist gas to reduce piled material through a homogeneous flux oriented at 180° with respect to the specimen [19]. The ablation parameters set to obtain the selected configurations are reported in Table 1.

Each titanium collector was fixed on a frame at a distance equal to the focal distance (160 mm) from the galvo head. Five repetitions for the same working parameters were carried out to study the laser cycle effects on channels configuration homogeneity in terms of width and depth distributions. The number of ablation loop was set to 30 to investigate the effect of the refund material on the grooves geometry.

Table 1. Designed laser-ablation cycles.

Parameter	Description	Equation	Set value
Area [mm^2]	Sample area	-	25
f [kHz]	q-switch frequency	-	30
P_{avg} [W]	Average power	-	2.64
v_s [mm/s]	Scan speed	-	304.8
d [mm]	Spot diameter	-	0.1
abs [%]	Absorption coefficient [18]	-	50
dc [%]	Duty cycle	-	30
dt [ns]	Pulse width	$dt = \frac{dc}{f}$	10^4
P_{peak} [W]	Peak power	$P_{peak} = \frac{P_{avg}}{f \cdot dt}$	8.80
t_{loop} [s]	Time per loop	$t_{loop} = 3\frac{Area}{d} \cdot \frac{1}{v_s}$	2.46
E_{pulse} [J]	Energy per pulse	$E_{pulse} = P_{peak} \cdot dt$	1.33
F_{pulse} [J/mm^2]	Fluence per pulse	$F_{pp} = abs \cdot \frac{4}{\pi d^2} \cdot E_{pulse}$	$5.6 \cdot 10^{-3}$
# loop	Number of loops	#	30

3. Pattern characterization

3.1. Optical microscope

The titanium samples surface was observed using the Mitutoyo Quick Scope QS-200z optical microscope system and the Zeiss LEO EVO 40 scanning electron microscope.

The optical images were used to analyze the details of the micro-patterns while the laser modification performed on an area of 25 mm^2 were evaluated by means of the SEM images. The samples showed a morphology sketched by the ablated configurations as shown in Fig. 3 and Fig. 4.

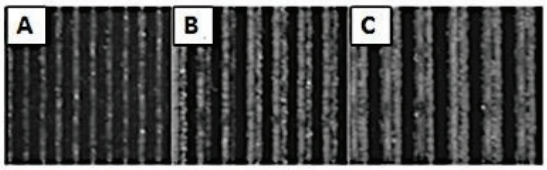

Fig. 3. Optical microscope images 2x of the configurations A, B and C for ES collector.

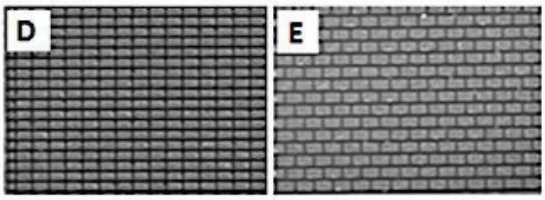

Fig. 4. Optical microscope images 2x of the configurations D and E for EDP collector.

3.2. Scanning electron microscope

The SEM images were processed with ImageJ software [20] to analyze the pattern dimensions (Fig. 5).

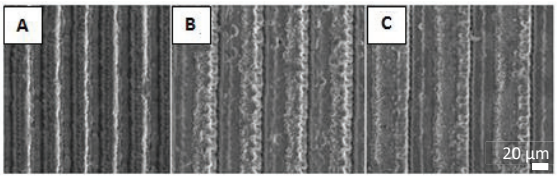

Fig. 5. SEM images 500x of pattern A, B and C.

Measures were taken considering all the grooves of the ablated area and the refund material that reconstitutes the channel cross-section. The channel wall exhibits a conical cross-section from the bottom to the top due to a great amount of refund material piled on the side of the marking line after each loop. The use of 30 ablation loops causes the presence of a certain quantity of vaporized material within the channel due to the high shape ratio chosen between line width and the reached depth.

Table 2 reports the data of the dimensional analysis performed on the SEM images that results in a difference between the imposed and the ablated pitch due to the overlapping of the 30 loops.

Table 2. Imposed pattern configurations by laser ablation of Titanium and resulting dimensions of the pattern.

Nominal pitch d_0(µm)	Channel pitch of Collector (µm)
25 (A)	23.5±1.7
50 (B)	47.3±2.0
75 (C)	70.4±2.4

Fig. 6 shows the SEM images of the configurations D and E used for the EDP collectors. Table 3 reports the data of the dimensional analysis performed on SEM images that results in similar dimensional differences as the configurations analyzed above.

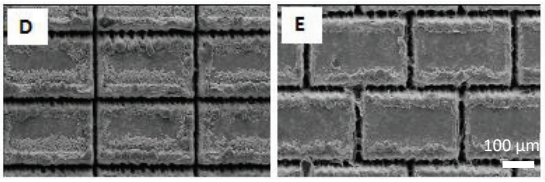

Fig. 6. SEM images 150X of patterns D and E.

Table 3. Imposed pattern configurations by laser ablation of Titanium and resulting dimensions of the pattern.

Nominal features l_0 (µm)	Collector features (µm)
125 (D)	126.1 ±0.8
250 (D)	252.2±0.9
125 (E)	127.4±0.7
250 (E)	253.5±0.8

3.3. Laser probe profilometer

The Mitaka PF-60 laser profilometer was used to investigate the cross sectional profile of the channels produced by the laser ablation. To better understand the role of the piles of refund material formed during the overlapping of the loops, a length of 500 µm on the surface of the sample A was analyzed (Fig.7).

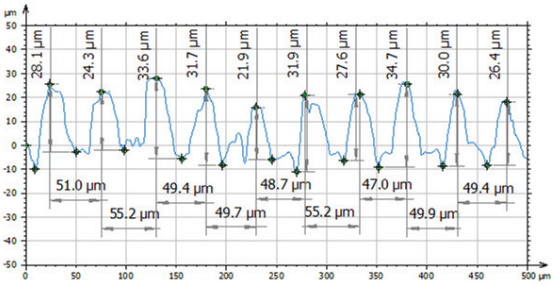

Fig. 7. Profile of the ablated configuration A.

As shown in Fig. 7 the refund material affects the geometry of the channels that have a conical shape along the depth.

4. Scaffold production

4.1. Electrospinning

Poly(ε-caprolactone) (PCL) with an average molecular weight of 80000 g/mol and porcine skin gelatin (GT) were both dissolved in formic acid. A solution of 40% PCL and a solution of 20% of gelatin were mixed at room temperature. A solution of 9:1 ratio of PCL:GT was prepared, stirred for 2 hours and poured into a 5 ml syringe equipped with a 0.8 mm needle. The detailed description of the electrospinning equipment is reported in [9]. The injection flow rate was set to 0.1 ml/h and the voltage was set at 20 kV for all the tests. The fibers were collected on the patterned collector with

configuration A, B and C located at 50mm from the tip of the needle.

4.2 Electrophoretic deposition

A solution of 0.1% (w/v) shrimp shell chitosan and rat-tail collagen was dissolved in acetic acid to obtain a 5:1 chitosan:collagen solution. The collector patterned with configuration D and E was used as cathode to obtain the scaffolds. The EPD was performed by using a power supply in potentiostatic conditions by applying a square waveform of 90 V for 25 seconds and 100 V for 5 seconds at pH 3. The process was run for 20 minutes to limit the effect of hydrogen bubbles inside the grooves [10].

5. Patterned scaffolds characterization

After the ES and EPD processes, the scaffolds were left overnight in NaOH 1M to allow an easy peeling off the collector.

SEM investigation allowed a complete morphological characterization of the sample surfaces as reported in Fig. 8.

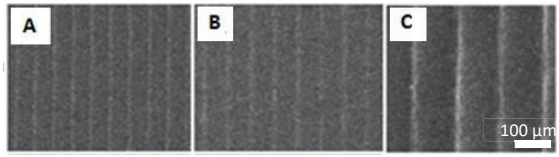

Fig. 8. SEM images 200x of the replicated patterns (configurations A, B and C) with a PCL gelatin ratio of 9:1.

For each test, the pattern dimensions were evaluated using the image processing software ImageJ [20]. In particular, the SEM images show that the channels are replicated in terms of linearity and definition at a tip-collector distance of 50 mm due to a better penetration of the fibers in the depth of the channel.

Table 4 reports the dimension of the pattern (30 replications) on the scaffold. It shows that the electrospun fibers are in general able to replicate the pattern geometry realized on the ablated collector. The bigger channels are most accurately replicated.

Table 4. Dimensions (Average ± Standard Deviation upon 30 replications) of the pattern replicated by the electrospun fibers.

Collector pitch (µm)	Channel pitch of the ES scaffold (µm)
23.5±1.8 (A)	25.9 ± 2.1
47.3±2.1 (B)	49.6 ± 3.1
70.4±2.4 (C)	75.3 ± 3.5

This is attributed to the fact that fibers along a wider range of directions can enter wider channels while, to enter the narrower channels the fibers have to be as much aligned and parallel as possible.

On the other hand, by the analysis of the SEM images of the EDP scaffolds (Fig. 9), it is possible to notice that both patterns were well replicated despite the presence of the pores due to hydrogen production, causing a control of the macro and micro porosity at the beginning of the EPD.

Table 5 reports the dimensions of the pattern (20 replications) on the scaffold. It shows that the deposited scaffolds are in general able to replicate the geometry of the pattern realized on the ablated collector despite the dimensional differences are not as negligible as in the case of the replications on the surface of the electrospun scaffolds.

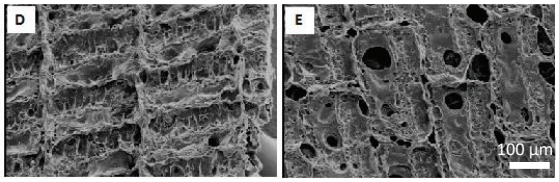

Fig. 9. SEM images 200x of the replicated patterns (configurations D and E) with a 5:1 chitosan collagen solution.

Table 5. Dimensions (average ± standard deviation upon 30 replications) of the pattern replicated by the electrodeposited solution.

Collector features (µm)	Features of the EDP scaffold (µm)
126.12 ±0.83 (D)	77.85 ± 8.83
252.23±0.91 (D)	188.44 ± 5.21
127.39±0.78 (E)	85.49±9.83
253.51±0.89 (E)	221.31±9.12

6. Cells attachment and orientation

Before cell seeding, all the scaffolds were sterilized with EtOH 70% solution for 30 min and UV light for 20 min and then washed with phosphate buffered saline (PBS). L6 rat myoblasts were seeded on the ES scaffolds while isolated human iPSC-cardiomyocites were used for the EDP scaffolds.

The samples were observed after 7 days of culture with an inverted fluorescent microscope and the organization of the cytoskeletal protein α tubulin and of the sarcomeric protein troponin T was evaluated to analyze the orientation of the cells onto the ES scaffolds and EDP scaffolds, respectively. In particular, the effects of the configurations A, B and C was evaluated on the basis of the orientation of the myoblasts while only the effect of the configuration D was analyzed by the evaluation of the cardiomyocites orientation. Fig. 10 shows that myoblast cells tend to spread in all directions in the absence of a pattern and are differently influenced by the geometry of the pattern.

The images point out the progressive decrease of cellular alignment as the replicated channel distance increases. In particular, L6 myoblasts seem to be more aligned along the configuration A of the pattern.

At the same way, the results reported in Fig. 11 show that without the pattern on the surface of the scaffold the cardiomyocites spread in all directions while when the pattern is adopted, the cells tend to regulate the cytoskeletal orientation according to the geometry of the grooves.

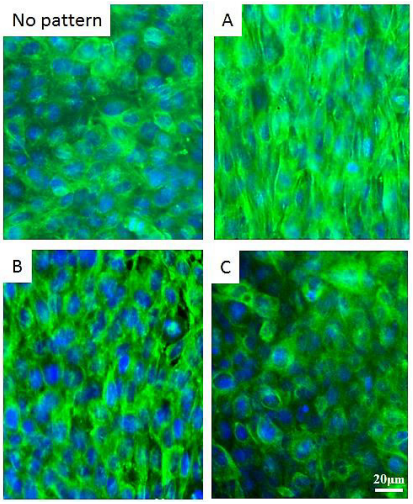

Figure 10. Fluorescent microscopy of L6 stained for α tubulin in green and DAPI in blue seeded onto the 9:1 scaffold without the pattern and with configuration A, B and C respectively.

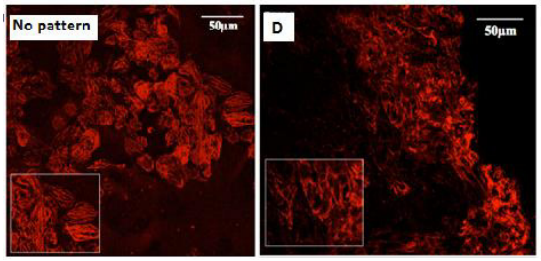

Fig.11. Fluorescent microscopy of human cardiomyocytes stained for cardiac troponin T in red seeded onto the EDP scaffold without and with D pattern respectively.

From these results, it can be demonstrated that configuration A on the scaffold can strongly influence the orientation of the cells according to the pattern direction. On the other hand, in case of configurations B, C and D, the orientation of the cells does not show significant symmetry or trend.

7. Conclusions

In this paper, laser ablated titanium collectors are used as templates during electrospinning and electrophoretic deposition tests to produce scaffolds with a surface topography that replicates the ablated micro-pattern geometry. Different configurations have been designed to be applied during the two production processes. The morphology of the templates on the collector has been evaluated. The dimensional differences between the imposed geometry and the ablated pattern were caused by the irregular shape of the ablated grooves due to the amount of refund material formed during the ablation process. Nevertheless, the imposed geometry was well represented on the surface of the collectors. The replications of the imposed geometry on the surfaces of the scaffolds have been analyzed and the geometry of the templates was in general well replicated onto the scaffolds. In particular, the dimensional differences between the imposed geometry and the replicated geometry on the EDP scaffolds were more significant compared to the case of the ES scaffolds probably due to the release of bubbles from the surface of titanium that leads to the formation of macro pores during this process. The natural micro architecture ensures the functional behavior of a certain tissue. In particular, the heart and skeletal muscles are composed by oriented fibers, therefore it was tested whether a surface pattern could be used to modify the orientation of muscle cells. Myoblasts were seeded on the ES scaffolds while cardiomyocytes were used on the EDP scaffolds. The results of the cell culture tests on the ES and EDP scaffolds confirm the strong influence of the pattern on cells orientation. According to the achieved results, the future researches will be focused on a more complete study of the quality of the replications in the case of different process parameters. Moreover, a statistical study of the orientation of the cells will be reported to give a quantitative description of what already evident in the fluorescent microscope images.

Acknowledgements

The authors would like to acknowledge the support and the assistance of Prof. Patrizia Dell'Era of University of Brescia.

References

[1] De Chiffre L, Kunzmann H, Peggs GN, Lucca D A. Surfaces in Precision Engineering, Microengineering and Nanotechnology. Annals of the CIRP 2003;52(2):561-77.
[2] Ginestra P, Ghazinejad M, Madou M, Ceretti E. Fabrication and characterization of polycaprolactone-graphene powder electrospun nanofibers. Proc of SPIE 2016;9932:Article number 99320A.
[3] Dhandayuthapani B, Yoshida Y, Maekawa T, Kumar DS. Polymeric scaffolds in tissue engineering application: a review. Int J Polym Sci 2011;Article ID 290602,19 pages.
[4] Hong H, Dong NG, Shi JW, Chen S, Guo C, Hu P, Qi H. Fabrication of a novel hybrid scaffold for tissue engineered heart valve. J Huazhong Univ Sci Technollog Med Sci 2009;29(5):599-603.
[5] Jana S, Tefft BJ, Spoon DB, Simari RD. Scaffolds for tissue engineering of cardiac valves, Acta Biomaterialia 2014;10:2877-93.
[6] Chien KR, Domian IJ, Parker KK. Cardiogenesis and the complex biology of regenerative cardiovascular medicine. Science 2008;322(5907):1494-7.
[7] Wang H, Shi J, Wang Y, Yin Y, Wang L, Liu J, Liu Z, Duan C, Zhu P, Wang C. Promotion of cardiac differentiation of brown adipose derived stem cells by chitosan hydrogel for repair after myocardial infarction. Biomaterials. 2014;35(13):3986-98.
[8] Salick MR, Napiwocki BN, Sha J, Knight GT, Chindhy SA, Kamp TJ, Ashton RS, Crone WC. Micropattern width dependent sarcomere development in human ESC-derived cardiomyocytes. Biomaterials 2014; 35(15):4454-64.
[9] Ginestra P, Ceretti, E, Fiorentino, A. Electrospinning of poly-caprolactone for scaffold manufacturing: experimental investigation on the process parameters influence. Proc. CIRP 2016;49:8-13.
[10] Benzoni P, Ginestra P, Altomare L, Fiorentino A, De Nardo L, Ceretti E, Dell'Era P. Biomanufacturing of a chitosan/collagen scaffold to drive adhesion and alignment of human cardiomyocyte derived from stem cells. Proc. CIRP 2016;49:113-20.

[11] Ceretti E, Ginestra PS, Ghazinejad M, Fiorentino A, Madou M. Electrospinning and characterization of polymer-graphene powder scaffolds, CIRP Annals 2017;66(1). In press.
[12] Yang D, Lu B, Zhao Y and Xia Y. Fabrication of aligned fibrous arrays by magnetic electrospinning. Adv. Mater. 2007;19:3802–6.
[13] Li D, Ouyang G, McCann JT and Xia YN. Collecting electrospun nanofibers with patterned electrodes. Nano Lett. 2005;5:913-6.
[14] Vaquette C and Cooper-White JJ. Increasing electrospun scaffold pore size with tailored collectors for improved cell penetration. Acta Biomater. 2011;7:2544-57.
[15] Dalton PD, Vaquette C, Farrugia BL, Gargaville T, Brown TD and Hutmacher DW. Electrospinning and additive manufacturing: converging technologies. Biomater. Sci. 2013;1:171-85.
[16] Rogers CM, Morris GE, Gould TWA, Bail R, Toumpaniari S, Harrington H, Dixon JE, Shakesheff KM, Segal J and Rose FRAJ. A novel technique for the production of electrospun scaffolds with tailored three-dimensional micro-patterns employing additive manufacturing. Biofabrication 2014;6(035003):1-11.
[17] Pérez N, Tavera T, Rodríguez A, Ellman M, Ayerdi I, Olaizola SM. Fabrication of submicrometric metallic hollow-core channels by laser interference lithography. Applied Surface Science 2012;258(23):9370-3.
[18] Giorleo L, Ceretti E, Giardini C. Optimization of Laser micro machining process for biomedical device fabrication. The International Journal of Advanced Manufacturing Technology 2015;82:901-7.
[19] Giorleo L, Ceretti E, Giardini C. Ti surface laser polishing: effect of laser path and assist gas. Proc. CIRP 2015;33:446-51.
[20] Rasband WS, ImageJ, U. S. National Institutes of Health, Bethesda, Maryland, USA, http://imagej.nih.gov/ij/, 1997-2014.